PNAS RESEARCH ARTICLE | EVOLUTION

Chromosomal inversions accelerate genetic evolution and drive ecological speciation across an island gradient

Ines Gómez-Ramos[a,1], Rogelio Sánchez-Villegas[b,1], Ashwini V. Mohan[c], Christophe Lavergne[d], José Cerca[e,f,g], José I. Márquez-Corro[b], André Marques[h], Santiago Martín-Bravo[b], Modesto Luceño[b], Kay Lucek[c,2], and Marcial Escudero[a,2]

Affiliations are included on p. 11.

Edited by Loren Riesberg, The University of British Columbia, Vancouver, BC, Canada; received February 9, 2026; accepted July 9, 2026 by Editorial Board Member Denis Duboule

Chromosomal rearrangements are hypothesized to facilitate speciation by suppressing recombination in locally adapted genomic regions, yet how they shape evolutionary rates during rapid divergence remains poorly understood. Here, we investigate the genomic architecture of two sister *Carex* (Cyperaceae) species on Réunion Island, which rapidly diverged (~0.5 Mya) to occupy contrasting tropical-montane and dry-subalpine habitats. Using chromosome-level assemblies and population genomics, we show that genomic divergence is not uniform across the genome but is concentrated within specific large-scale inversions. Crucially, genes within these structural variants exhibit significantly accelerated rates of protein evolution, as evidenced by elevated ω, compared to the collinear genome. This is consistent with recombination suppression and subsequent relaxation of purifying selection driving these patterns, which may complement or even outweigh the signal of positive selection. Functional analysis and environmental associations reveal that these "genomic accelerators" include key adaptive loci: Inversions on chromosomes 14 and 28 are enriched for mechanosensitive ion channels and auxin transport, which is consistent with facilitating the interspecific physiological shift to aridity. Partial redundancy analyses reveal that ongoing intraspecific ecological adaptation is highly polygenic across the collinear genome. Our results demonstrate that genomic architecture actively dictates evolutionary speed, suggesting that certain lineages boosted by structural variants may bypass the typical constraints of purifying selection to rapidly exploit vacant ecological opportunities.

speciation | evolution | island | inversion | genomics

Significance

This study demonstrates that large-scale genomic inversions can act as critical engines of evolutionary divergence. We reveal that genomic divergence is disproportionately concentrated within these structural variants, where genes exhibit significantly accelerated protein evolution. Crucially, we show that this acceleration is driven by recombination suppression and relaxed purifying selection, challenging the paradigm that rapid divergence is solely driven by positive selection. This highlights how structural architecture can enable lineages to bypass standard evolutionary constraints. Furthermore, we link this genomic architecture directly to physiological adaptation, showing that these inversions are enriched for mechanosensitive ion channels essential for surviving shifts to aridity. Ultimately, our findings provide a unified framework connecting structural variation, relaxed selection, and ecological adaptation.

While speciation is a fundamental evolutionary process, our knowledge of the genomic underpinning of rapid diversification remains limited beyond a few model systems (1–3). Understanding the genomic architecture of rapid ecological diversification provides general insights into how species may adapt in a rapidly changing world, a task now facilitated by the increasing availability of genomic and bioinformatic tools (4). To this end, isolated systems such as volcanic islands are invaluable; they allow for the study of speciation processes in situ without the complicating factors of recurrent extrinsic gene flow (5, 6). The importance of these insular systems was historically anchored by observations in the Galapagos and Mascarene Islands (the later being home to the dodo, *Raphus cucullatus*), which served as foundational sites for defining biological concepts of evolution and speciation (7) and extinction (8, 9), respectively.

Oceanic islands have long been considered ideal natural laboratories to study evolution in action (10, 11). Due to their geological dynamism and distinct ecological opportunities, these isolated environments frequently promote rapid speciation and lineage diversification by exploiting different available niches (6). In some cases, this process leads to species radiations, whereby numerous species evolve from a common ancestor in a short period of time (12–14). The most famous example of species radiation on volcanic islands in response to different ecological niches are the Galápagos or Darwin's finches, which evolved different beak shapes to use different seeds (15, 16). Textbook examples of island radiations in plants include silverswords in Hawaii (17), *Echium* in Macaronesia (18) and *Scalesia* in the Galápagos Islands (19). While recent genomic approaches have advanced the phylogenetic resolution of island radiations (19, 20), much less is known about the genomic signatures characterizing the early stages of rapid speciation (14, 21–23). Young oceanic islands such as the Réunion island [2.1 Mya (24)] are ideal systems to study recent speciation processes and its genomic drivers.

Many rapid island speciation events have been linked to chromosomal rearrangements (25, 26). Chromosomal rearrangements such as inversions, translocations, fissions and

The authors declare no competing interest.

This article is a PNAS Direct Submission. L.R. is a guest editor invited by the Editorial Board.

[1]I.G.-R. and R.S.-V. contributed equally to this work.

[2]To whom correspondence may be addressed. Email: kay.lucek@unine.ch or aescudero2@us.es.

This article contains supporting information online at https://www.pnas.org/lookup/suppl/doi:10.1073/pnas.2604805123/-/DCSupplemental.

Published August 12, 2026.

fusions are often associated with phenotypic differences (27, 28). Among these, inversions have received particular attention, as they can protect adaptive gene combinations from recombination (29–31). While genetic differences often accumulate following speciation, chromosomal rearrangements can actively promote initial divergence by creating localized barriers to introgression in regions under divergent selection (32, 33). Chromosomal rearrangements may promote speciation, either by causing hybrid dysfunction especially in plants (27, 34) and/or through suppression of recombination between locally adapted genes or supergenes (35). Large-scale rearrangements may especially establish in holocentric species, which lack a single centromere, as they are predicted to be initially more tolerated (36).

Here, we examine a case of rapid island speciation between the two holocentric sister species *Carex boryana* Schkuhr and *Carex borbonica* Lam., the latter being endemic to Réunion Island. This species pair offers a window into the divergence mechanisms that drive plant speciation in island ecosystems. Both species constitute a clade of very recent origin, resulting from a single colonization event of Réunion [ca. 0.5 Mya (37)]. Réunion is a volcanic island that is hypothesized to have emerged approximately 2.1 Mya (24). The high-altitude subalpine belt—the habitat of *C. borbonica*—is a much younger environment that emerged only 0.55 Mya for Piton des Neiges and Le Maïdo and 0.36 Mya for Piton de la Fournaise (38). This suggests that divergence of this species pair could have been triggered by the emergence of a novel ecological niche. Despite the short evolutionary time, the two species display extremely divergent morphologies and niches. *Carex boryana* occurs in tropical montane wet forests and other shady places (1,300 to 2,350 m.a.s.l.) of Réunion Island. This species also occurs on Mauritius Island, where it is very rare (39). The morphology (Fig. 1 *A* and *C*) of *C. boryana* resembles the typical giant morphology of other closely related *Carex* species dwelling in similar humid tropical habitats in the mountains of eastern tropical Africa (39, 40). *Carex borbonica* only occurs in the subalpine belt of Réunion Island, in dry, sunny and sandy places on volcanic soils at higher altitudes (2,250 to 2,400 m.a.s.l.). It is typically much smaller than *C. boryana* and shows coriaceous leaves and erect or suberect female spikes (Fig. 1 *B* and *D*). Phenotypically intermediate individuals have been reported in the clinal zone between the two habitats (Fig. 1 *E* and *F*), which have been postulated as hybrids (40). Both species and intermediate individuals show the same karyotype and meiosis pairing [$2n = 34^{II} = 68$ (41)], but smaller chromosomal rearrangements such as inversions or translocations distinguishing both species may exist.

Combining state-of-the-art genomic and ecological analyses, we aim to unravel the genomic processes underlying diversification and ultimately speciation through rapid local adaptation in an island ecosystem. Specifically, we ask i) whether patterns of genomic divergence in response to ecological differentiation are distributed across the whole genome or discrete in few localized regions ii) are there genomic islands of increased differentiation associated with chromosomal rearrangements (i.e., inversions) that suppress recombination in those regions? iii) are rearrangements relevant for ecological differentiation even in the presence of interspecific gene flow? We hypothesize that genomic divergence is discrete and limited to specific genomic regions associated with rearrangements that suppress recombination locally.

Results

Genome Assembly and Annotation Results. The genomes of *C. boryana* and *C. borbonica* were sequenced on a PacBio Revio, yielding a total of 70.8 Gb HiFi reads for *C. boryana* (~180× coverage) with a mean read length of 18,427.9 bp and 64.5 Gb for *C. borbonica* (~160× coverage) with a mean read length of 16,302.6 bp. The initial de novo assembly with hifiasm produced primary contig assemblies of 436.2 Mb and 444.6 Mb, respectively. Haplotigs were successfully purged using HifiASM and purge_dups, resulting in a final purged primary assembly size of 388.8 Mb for *C. boryana* and of 387.6 Mb for *C. borbonica*.

Chromosome-level scaffolding was achieved using Hi-C proximity ligation data, yielding a total of 68.91 Gb of highly accurate reads for *C. boryana* (~172× coverage) and 57.2 Gb for *C. borbonica* (~143× coverage). The final scaffolds captured 99.56% and 98.94% of the total sequence for *C. boryana* and *C. borbonica*, respectively, in 34 scaffolds, corresponding to the expected number of chromosomes for both species [$2n = 34^{II} = 68$ (41)]. The final scaffold N50 increased dramatically to 11.17 Mb and 11.19 Mb. Whole-chromosome Hi-C contact maps confirmed the structural integrity and high contiguity of these 34 primary scaffolds for both *C. boryana* (*SI Appendix*, Fig. S1) and *C. borbonica*

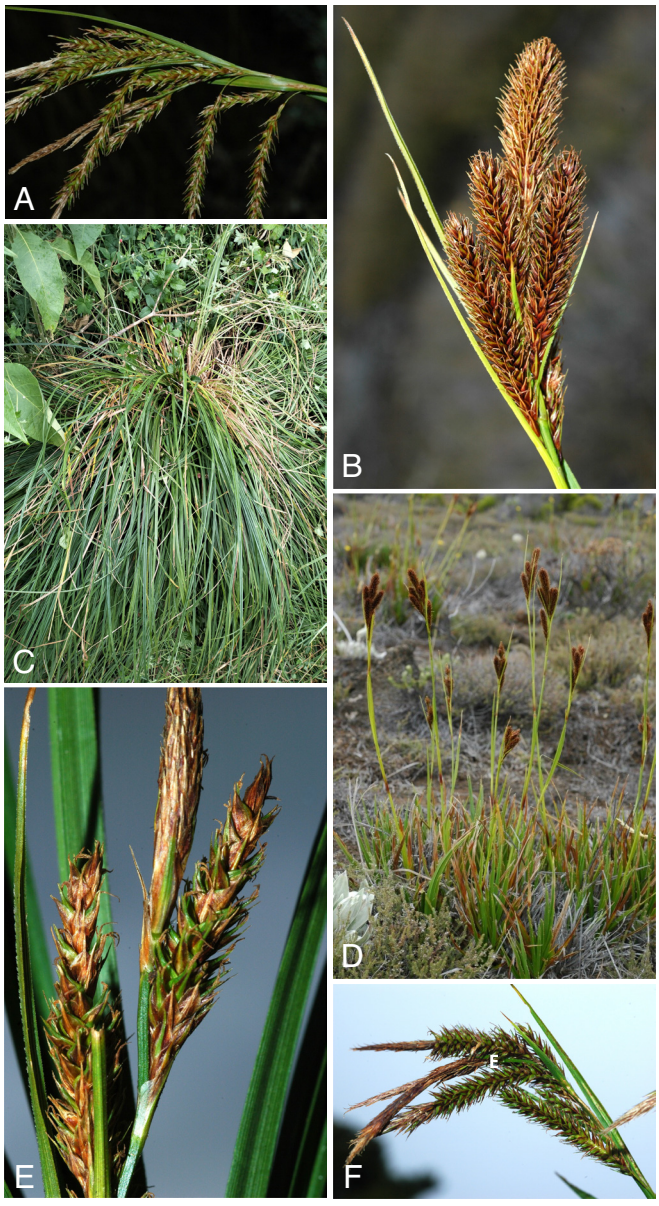

Fig. 1. (*A*) Typical inflorescence of *C. boryana*. (*B*) Typical inflorescence of *C. borbonica*. (*C*) Typical habit of *C. boryana*. (*D*) Typical habit of *C. borbonica*. (*E*) Inflorescence of an individual of *C. borbonica* with *C. boryana* introgression. (*F*) Inflorescence of an individual of *C. boryana* with *C. borbonica* introgression.

(*SI Appendix*, Fig. S2), displaying continuous diagonals and lacking off-diagonal breaks characteristic of misassembly. Quality metrics confirmed high confidence: Genome completeness, assessed with compleasm against the Poales ODB10 lineage, showed for both genomes 98.04% complete BUSCOs, achieving a high assembly quality values (Merqury QV of 75.34 and 71.84 for *C. boryana* and *C. borbonica*, respectively). Contaminant scaffolds were identified and removed using Tiara prior to final filtering. Remaining unanchored scaffolds (all < 1 Mb) were excluded from the primary assemblies. Telomeric repeat identification (TIDK) confirmed that these minor, unplaced fragments overwhelmingly consisted of unassembled, highly repetitive satellite arrays and telomeric tandem repeats (*SI Appendix*, Figs. S3 and S4).

For annotation, repeat elements were first identified and soft-masked to facilitate accurate gene prediction by BRAKER3 (42). Repeats were subsequently classified using the Earlgrey pipeline (43). Interspersed repeats constituted 60.2% of the *C. boryana* genome (25.2% unclassified), primarily LTRs (14.98%), satellite DNAs (10.32%) and LINEs (4.40%) (*SI Appendix*, Fig. S5). For *C. borbonica*, interspersed repeats constituted 60.0% of the genome (26.47% unclassified), also primarily comprising LTRs (16.23%), satellite DNAs (10.14%) and LINEs (3.20%) (*SI Appendix*, Fig. S62). No differences in TE composition or prevalence was observed between species. The BRAKER3 pipeline resulted in the prediction of 29,665 and 28,123 high-confidence protein-coding genes for *C. boryana* and *C. borbonica*, respectively.

Synteny Analyses. The comparative genomic analysis with GENESPACE (44) revealed a defined set of structural variations between the two species (*SI Appendix*, Fig. S7). Only a single large translocation event was identified between chromosome 4 of *C. boryana* and chromosome 10 of *C. borbonica* (this potential translocation between chromosomes 4 and 10 is characterized by unique repeat DNA patterns and numerous uncharacterized proteins). Two large inversions on chromosomes 14 (INV14.1) and 18 (INV18.2) could be clearly detected and five smaller inversions were identified on chromosomes 3 (INV3.4), 20 (INV20.3), 22 (INV22.17), 28 (INV28.20), and 32 (INV32.16) (*SI Appendix*, Table S2).

The synteny alignment identified 294 blocks larger than 10 kb (*SI Appendix*, Fig. S8). The majority of the aligned genome (176 syntenic blocks, 59.9%) remained syntenic (SYN) and constituted 98.5% of the genome, indicating large regions of collinearity between the two assemblies. The remaining syntenic blocks consisted of structural rearrangements that constituted only 1.5% of the genome. Among the detected structural variants (SVs), inversions were the most frequent, accounting for 93 events, or ~78.8% of all nonsyntenic structural changes. These inversions included simple inversions (INV, 34 events, 11.6% of all events), inversions with a duplication (40 events, INVDP, 13.6%), and inversions with a translocation (INVTR, 19 events, 6.5%). Duplications (DUP) represented 7.8% (23 events) of rearranged synteny blocks, while simple translocations (TRANS) were the rarest, totaling only 0.7% (2 events).

The 30 largest SVs (*SI Appendix*, Table S2) further highlighted the dominance of large-scale inversions in distinguishing the two genomes. The largest SV was a simple inversion (INV) of 2.29 Mb located on chromosome 14 (INV14.1), followed by a 861.9 kb inversion on chromosome 18 (INV18.2). The largest complex SVs were inversions with translocation (INVTR) events on chromosome 11 (INVTR11.5 and INVTR11.6 with 234.9 kb and 221.6 kb, respectively). The largest duplication (DUP) measured 204.5 kb (the 7th largest rearrangement or DUP2.7) on chromosome 2 and the largest inversion duplication (INVDUP) event measured 179.4 kb on chromosome 3 (INVDP3.10). These regions are often clustered, with the majority of the large DUPs and INVDUPs appearing on chromosomes 2 and 3 (*SI Appendix*, Table S2). Overall, only one simple 137.8 kb translocation (TRANS) was within the 30 largest SVs on chromosome 3 (TRANS3.12).

To validate the structural variants and rule out potential scaffolding artifacts, we examined the reciprocal Hi-C cross-mapping contact maps. The mapping of *C. borbonica* Hi-C reads onto the *C. boryana* reference genome (and vice versa) confirmed the major inversions. Specifically, the characteristic off-diagonal interaction signatures were prominently visible at the genomic coordinates of the largest identified inversions, including INV14.1, INV18.2, INV20.3, INV3.4, INV32.16 and INV28.20 (*SI Appendix*, Figs. S9 and S10).

Whole Genome Genotyping, Variant Calling and Filtering, and Phylogenetic Analysis. Whole-genome resequencing data were generated for 186 samples from 37 locations across Réunion Island (Fig. 2) and six outgroup accessions (*C. laevigata* and *C. helodes*), amounting to a total of 192 samples with an estimated coverage depth of 25×. Two individuals were omitted due to data missingness (*SI Appendix*, Table S3). The final filtered dataset for population genomic analyses consisted of 184 individuals (59 of *C. borbonica*, 102 *C. boryana* and 23 putatively introgressed/hybrid). Alignment to the *C. boryana* reference genome and joint variant calling, followed by filtering yielded 3,054,020 polymorphic SNPs.

A maximum likelihood (ML) phylogenetic inference was performed on 2,675,290 strictly variable SNPs (see *SI Appendix, Supplementary Materials and Methods* for details), utilizing a General Time Reversible (GTR) model with Ascertainment Bias Correction (ASC) to account for the use of only variable sites. The resulting phylogenetic topology (Fig. 2) exhibited exceptionally high statistical support (*SI Appendix*, Fig. S11). Branch support value is 95% bootstrap or higher for gray dark branches and lower than 95% for dashed light gray branches (which are very exceptional). Branch support values, derived from an ultrafast bootstrap (UFBoot2) and a Shimodaira–Hasegawa-like approximate likelihood ratio test (aLRT), were consistently near 100 across most nodes (81.28% showed a 100/100 support) and only terminal nodes grouping individuals from the same populations showed lower support (*SI Appendix*, Fig. S11). This outcome confirms the robustness of the inferred phylogenetic structure splitting *C. boryana* and *C. borbonica*. Phylogenetically 70 individuals were identified as *C. borbonica* and 114 as *C. boryana* (Fig. 2). Based on phylogenetic position and/or long branch lengths, some samples show signals of potential interspecific introgression (Fig. 2 and *SI Appendix*, Fig. S11). In two cases individuals from the same location fell into the two main clades that correspond to each of the two species (16JMC17_1 vs. 16JMC17_2 and 20ML09_7 vs. the rest 20ML09; *SI Appendix*, Fig. S11).

Population Genetic Diversity and Differentiation. To determine the impact of large SVs on genomic differentiation and diversity, we performed Mann–Whitney *U* tests comparing windows inside all large SVs (>10 kbp, N = 4,878 windows) against all non-SV windows (N = 324,088) (*SI Appendix*, Fig. S12). The results indicate significant differences for all metrics where differentiation (F_{ST}) inside SV was higher (Mean F_{ST} = 0.4505) compared to the non-SV background (Mean F_{ST} = 0.4057, $P < 0.001$). We also found a significant increase of d_{xy}, within SVs (Mean = 0.0035) compared to the non-SV background (Mean = 0.00347, $P < 0.001$). Conversely, nucleotide diversity (π) was significantly reduced within SVs in both populations: $\pi_{borbonica}$ decreased from 0.0015 (Non-SV)

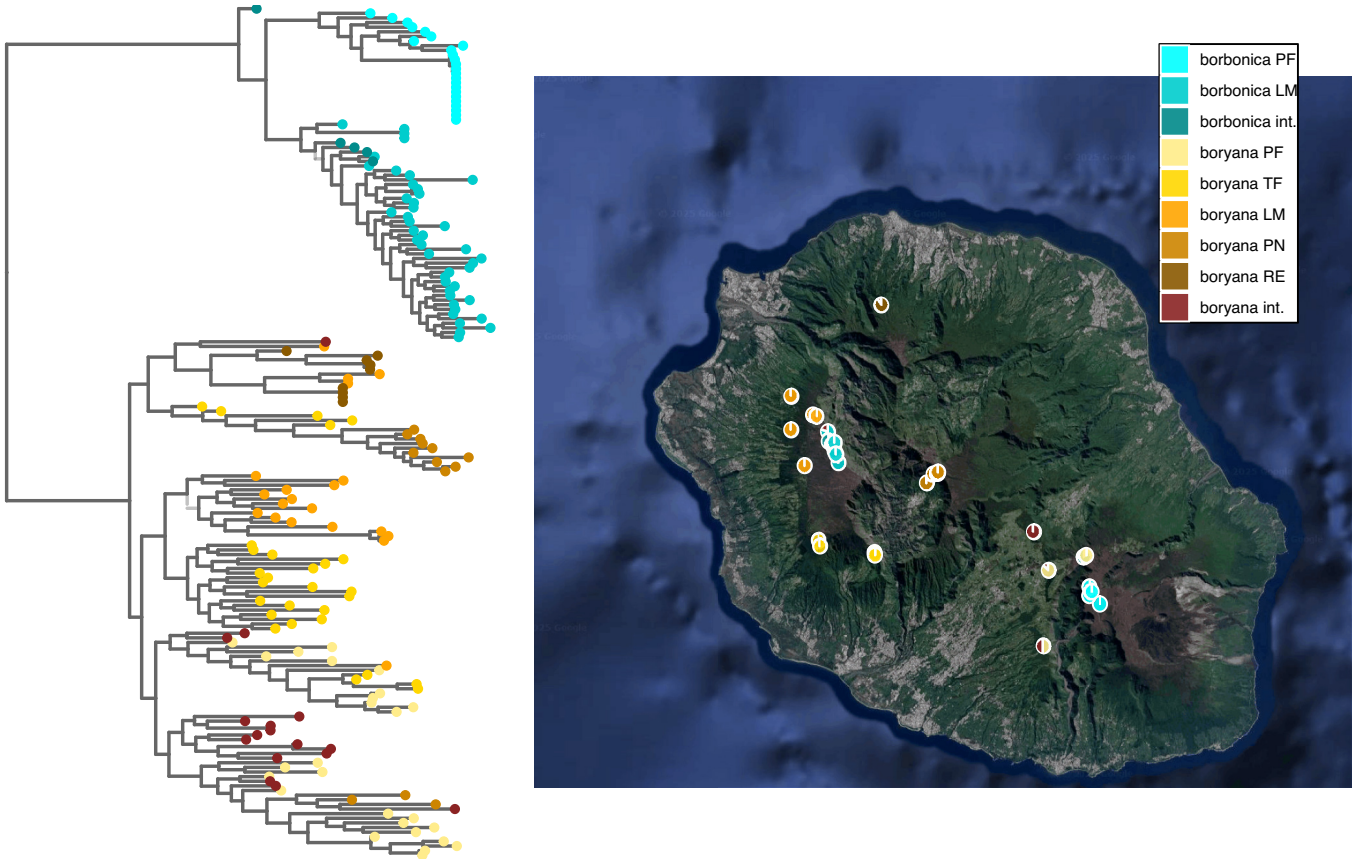

Fig. 2. To the left, maximum likelihood phylogenetic inference of *C. boryana* and *C. borbonica* based on SNP data. The phylogenetic tree was reconstructed using the Maximum Likelihood (ML) method implemented in IQ-TREE from an alignment of 2,675,290 variable SNP sites. The analysis employed the GTR + ASC (General Time Reversible model with Ascertainment Bias Correction) to account for the use of only strictly variable sites. Topology in dark gray has a bootstrap support of 95% or higher and topology in dashed light gray has a support of lower than 95%. To the right, satellite image map of Réunion Island. Populations are represented by piecharts with pure *C. borbonica* in cyan tonalities depending on the area of origin (from lighter to darker: borbonica PF = *C. borbonica* from the area of Piton de la Fournaise, and borbonica LM = *C. borbonica* from the area of Le Maïdo), introgressed *C. borbonica* in dark cyan, pure *C. boryana* in orange tonalities depending on the area of origin (from lighter to darker: boryana PF = *C. boryana* from the area of Piton de la Fournaise, boryana TF = *C. boryana* from the areas of Foret du Tevelave and Fenêtre des Makes, boryana PN = *C. boryana* from the area Piton des Neiges, boryana RE = *C. boryana* from the area Réserve Naturelle de la Roche Écrite, and boryana LM = *C. boryana* from the area of Le Maïdo) and introgressed *C. boryana* in dark brown.

to 0.0013 (SV, $P < 0.001$), with $\pi_{boryana}$ showing a similar trend (P =0.036). Furthermore, the ratio of diversity ($\pi_{borbonica}/\pi_{boryana}$) was significantly lower inside SVs (Mean = 1.2875) compared to the background (Mean = 1.4587, $P < 0.001$). The simple linear models of rearrangements >10 kb (N =104), indicate that the average F_{ST} of the rearrangements is significantly explained by the d_{xy}, as a proxy of the age of the rearrangement (df = 102, adjusted R^2 = 0.094, F = 11.64, P = 0.000927, AIC = −115.5), and by the size of the rearrangement (df = 102, adjusted R^2 = 0.039, F = 5.188, P = 0.0248, AIC = −109.4), with the complex linear model being the best supported one (df = 101, adjusted R^2 = 0.140, F = 9.418, P = 0.000178, AIC = −120.0).

The strongest signal is the increased divergence reflected in F_{ST} within large inversions: six of the largest inversions (INV14.1, INV18.2, INV20.3, INV3.4, INV32.16 and INV28.23, Fig. 3, Table 1, and *SI Appendix*, Figs. S4 and S13–S17), ranging up to 2.29 Mbp (INV14.1) (Mann–Whitney U test, all $P < 0.001$). These six SVs exhibited increased F_{ST}, while most other SV types (e.g., duplications, translocations) did not show a higher F_{ST} (*SI Appendix*, Table S4). Regarding the six SVs with significantly heightened F_{ST} compared to the genomic background, INV14.1, INV18.2, INV20.3, INV3.4 and INV32.16 showed a significant difference in the distribution of $\pi_{borbonica}$ (significantly smaller within SV versus outside), only INV20.3 and INV3.4 showed a significant difference in the distribution of $\pi_{boryana}$ (significantly smaller within SV versus outside), and INV14.1, INV18.2, INV20.3, INV3.4 and INV32.16 showed significant differences in the $\pi_{borbonica}/\pi_{boryana}$ ratio (significantly smaller within SV versus outside). Twenty-three of the 26 SVs analyzed (four small SVs, INVDP2.13, DUP2.18, DUP2.19, INVDP2.21, were excluded from the statistical tests as they contained fewer than the minimum required five 1,000 bp windows) showed a significant difference in the distribution of $\pi_{borbonica}$ ($\pi_{borbonica}$ smaller within SV than outside), 19 of the 26 SVs analyzed showed a significant difference in the distribution of $\pi_{boryana}$ ($\pi_{boryana}$ smaller inside SV than in the background), and 14 SVs showed significant differences in the $\pi_{borbonica}/\pi_{boryana}$ ratio ($\pi_{borbonica}/\pi_{boryana}$ smaller within SV than in the background).

To confirm that these patterns were not an artifact of the window-based estimation (45), we reevaluated differentiation using a SNP based F_{ST} approach across the total dataset of 3,054,020 SNPs. This per-SNP analysis confirmed that differentiation is significantly higher within structural rearrangements than in the collinear background (Mean F_{ST_inside} = 0.303, Mean $F_{ST\_outside}$ = 0.284, Mann–Whitney U, $P < 0.0001$). Notably, the large simple inversions showed the strongest signals of enrichment for high-F_{ST} outliers (defined as the top 1% of all SNPs; F_{ST} > 0.983). The inversion on chromosome 14 (INV14.1) exhibited an eightfold enrichment of these outliers (8.01%), and the inversion on chromosome 20 (INV20.3) showed a 13-fold enrichment

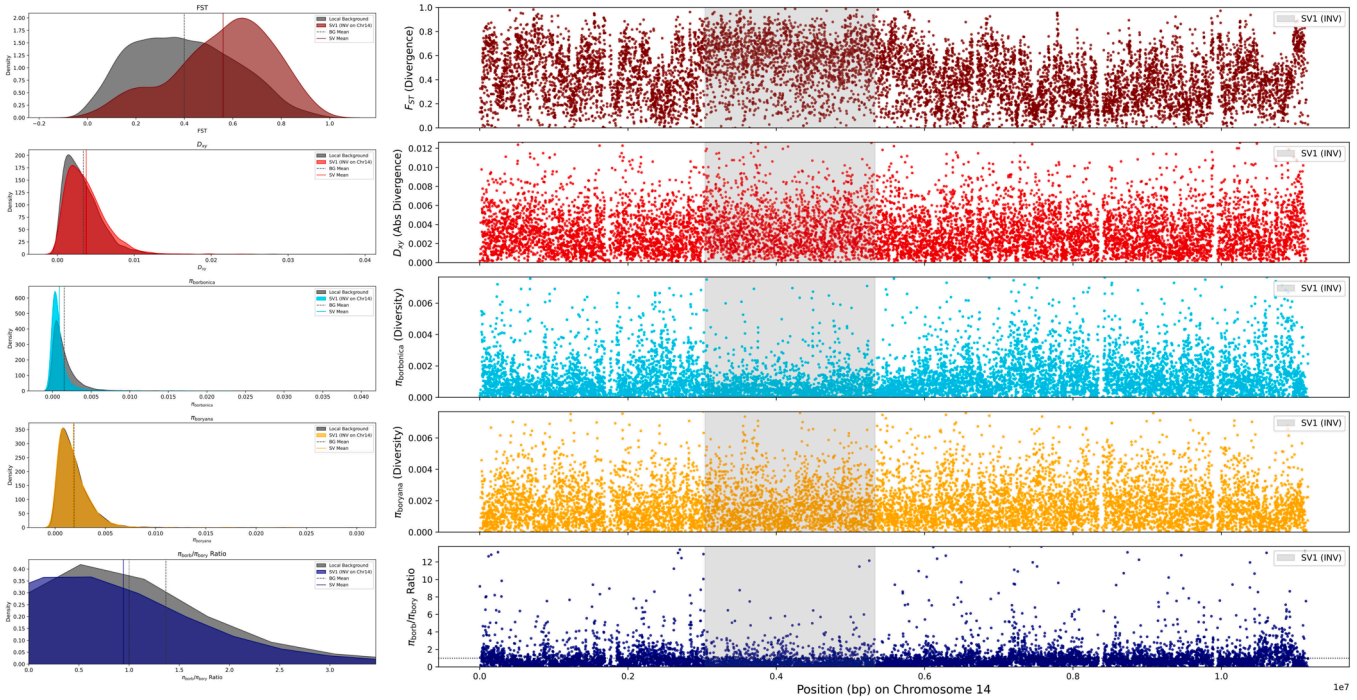

Fig. 3. To the left, distributions of genomic windows of 1,000 bp containing estimates of Weir and Cockerham's F_{ST} (in maroon), d_{xy} (in red), *C. borbonica* nucleotide diversity π_{Pop1} (in cyan), *C. boryana* nucleotide diversity π_{Pop2} (in orange), and the π_{Pop1}/π_{Pop2} ratio (in blue) for the inversion on chromosome 14 (colored) against the background (gray). To the right, values genomic windows of 1,000 bp containing estimates of Weir and Cockerham's F_{ST} (in maroon), d_{xy} (in red), *C. borbonica* nucleotide diversity π_{Pop1} (in cyan), *C. boryana* nucleotide diversity π_{Pop2} (in orange), and the π_{Pop1}/π_{Pop2} ratio (in blue) for the chromosome 14. Inversion indicated by a transparent gray window.

(13.12%), while the one on chromosome 32 (INV32.16) showed over sixfold enrichment (6.47%). In contrast, other large rearrangements showed no such spike in differentiation. For instance, the large inversions on chromosome 18 (INV18.2) and chromosome 3 (INV3.4) showed enrichment levels below or near the genomic background (0.34% and 0.11%, respectively), and the inversion on chromosome 28 (INV28.23) showed no enrichment (*SI Appendix*, Table S5).

Linkage Disequilibrium. To determine if the large structural variants suppress recombination and restrict localized gene flow, we analyzed patterns of linkage disequilibrium (LD) decay in 30 largest SVs (*SI Appendix*, Fig. S18 and Table S6). The six inversions with significantly elevated per-window F_{ST} (INV14.1, INV20.3, INV3.4 and INV32.16 Wilcoxon signed-rank test, $P < 0.001$; INV18.2 and INV28.23, $P < 0.05$; *SI Appendix*, Fig. S18) exhibited significantly elevated LD compared to their collinear chromosomal backgrounds across matched physical distances. Two additional inversions without significantly elevated per-window F_{ST} (INV18.22, and INV18.24) showed statistically significant elevations in LD ($P < 0.001$).

Population Structure Analyses. After filtering and LD pruning, 827,809 single nucleotide polymorphisms (SNPs) for 184 samples were retained for analysis. Cross-validation (CV) in ADMIXTURE identified K = 8 as the best supported number of clusters. They show two clear ancestry groups within *C. boryana* (mostly three different clusters out of eight) and *C. borbonica* (mostly five different clusters out of eight) with limited (all except one individual <5%) mixed ancestry between the two species in six individuals out of 70 phylogenetically identified as *C. borbonica* and 15 individuals out of 114 phylogenetically identified as *C. boryana*. When using SNPs within inversions, a higher number of clusters was better supported (*SI Appendix*, Fig. S19): i) K = 11 for INV14.1 (4,542 encompassing SNPs), K = 10 for INV18.2 (1984 SNPs) and K = 14 for INV20.3 (532 SNPs), INV3.4 (434 SNPs), INV32.16 (256 SNPs) and INV28.23 (172 SNPs). The degree of mixed ancestry for INV14.1 was highly restricted;

Table 1. Evolutionary divergence within top SVs vs. local background

SV ID	Type	Chr	Size (kb)	N (SV/BG)	F_{ST}	d_{xy}	π_{borb}	π_{bory}	Ratio (π_{borb}/π_{bory})
INV14.1	INV	14	2291.8	1,956/7,730	0.560**	0.0038**	0.0009**	0.0018 (0.355)	0.94**
INV18.2	INV	18	861.9	723/8,224	0.419**	0.0031 (0.986)	0.0014**	0.0018 (0.065)	1.21**
INV20.3	INV	20	267.5	225/9,019	0.630**	0.0044**	0.0009**	0.0017*	1.05**
INV3.4	INV	3	235.5	202/12,442	0.467**	0.0032*	0.0009**	0.0019*	1.04**
INV32.16	INV	32	127.3	117/6,468	0.587**	0.0038**	0.0008**	0.0017 (0.315)	1.70**
INV28.23	INV	28	80.4	75/7,401	0.459*	0.0034 (0.102)	0.0014 (0.405)	0.0018 (0.374)	0.93 (0.523)

Comparison was made using the Mann–Whitney *U* test between windows (1 kbp) fully within the SV region and windows on the same chromosome outside the SV (local background, BG). N indicates the number of windows used for the comparison (SV/BG). *P*-value interpretation: (*P*-value) values in parentheses are nonsignificant. * indicates $P < 0.05$. ** indicates $P < 0.001$. F_{ST} was tested for enrichment (SV > BG). π_{borb} and π_{bory} metrics and $\pi_{borb}\backslash\pi_{bory}$ ratio were tested for difference (SV = BG). Only the six major SVs with significant differences in F_{ST} are shown, the remaining major SVs are shown in *SI Appendix*, Table S3. *P*-values are not corrected for multiple testing.

the region appeared nearly fixed between the two species, with the exception of a single heterozygous *C. borbonica* individual, displaying ~50% mixed ancestry and only trace admixture (~1%) in three *C. boryana* individuals (Fig. 4). INV18.2 and INV20.3 similarly displayed distinct ancestry, consistent with a near-fixation between the species, with only a single exception for a *C. borbonica* individual and INV18.2, which shows a higher mixed ancestry (*SI Appendix*, Fig. S19). In contrast, several inversions exhibited active segregation, though the architecture of this mixed ancestry varied (*SI Appendix*, Fig. S19). Notably, INV3.4 is highly polymorphic within *C. boryana*, containing three possible heterozygotes as well as four homozygotes that exhibit entirely *C. borbonica* ancestry. Crucially, aside from these specific individuals, admixture within INV3.4 is virtually nonexistent, indicating that this inverted region segregates across populations as an entire genomic block. INV32.16 similarly showed very limited admixture overall, capturing only a single putative heterozygote within *C. borbonica*. Conversely, INV28.23 demonstrated a higher overall degree of mixed ancestry; in addition to capturing three possible heterozygotes in *C. boryana*, this region exhibited more diffuse, low-level admixture across multiple individuals, suggesting a slightly more permeable genomic block. To highlight mixed ancestry, we plotted K = 2 for both the genome-wide dataset and the focal inversions (*SI Appendix*, Fig. S20). However, these results should be interpreted with caution, as restricting the model to K = 2 tends to artificially overestimate the degree of mixed ancestry.

Introgression Analyses. To test the hypothesis that structural variants (SVs) influence genomic differentiation between *C. boryana* and *C. borbonica*, we quantified introgression using Patterson's D and fd statistics (*SI Appendix*, Table S7). While the genomic background exhibits a signal of significant, but low-level, bidirectional introgression (fd_background = 0.007 to 0.019; $P < 0.0001$), we found that the majority of identified SVs act as potent localized barriers to gene flow. Inversions INV14.1, INV18.2, INV20.3, INV32.16, and INV28.23 consistently demonstrated introgression proportions (fd) near zero, often falling below the background rate. Notably, for INV18.2, INV20.3, and INV32.16, introgression was statistically indistinguishable from zero in the *C. boryana* to *C. borbonica* direction ($P > 0.13$), indicating that these structural arrangements effectively protect from genomic swamping through background hybridization. In stark contrast, INV3.4 emerged as a significant outlier among the analyzed structural variants. Unlike the barrier-like behavior of other inversions, INV3.4 showed a localized spike in introgression (D = 0.445, fd = 0.109, $P = 0.0001$).

Landscape Genomics. A Redundancy Analysis (RDA) revealed a significant relationship between genetic variation and the five selected bioclimatic variables (BIO1 Annual Mean Temperature, BIO4 Temperature Seasonality, BIO12 Annual Precipitation, BIO14 Precipitation of Driest Month, and BIO16 Precipitation of Wettest Quarter). The overall model was statistically significant (ANOVA: df = 5, F = 23.506, $P = 0.001$), explaining 39.77% of the total genetic variance (Constrained Inertia = 969.6 out of Total Inertia = 1317.0). The remaining 60.23% was attributed to unconstrained variance (bioclimatic variables principal components). The first constrained axis accounted for 76.81% of the total variation of the constrained inertia (or 30.55% of the total genetic variance), while the second axis captured 9.86% of the constrained inertia (or 3.92% of the total genetic variance) (Fig. 5). Marginal effect tests demonstrated that all five bioclimatic predictors significantly explained genetic variation (all $P = 0.001$), with Precipitation of Driest Month (BIO14) showing the strongest explanatory power (df = 1, F = 12.686, $P = 0.001$) followed by Precipitation of Wettest Quarter (BIO16, df = 1, F = 6.891, $P = 0.001$). Resulting in a clear separation of individuals of each species primarily driven by the strong environmental gradients represented by the constrained axes (Fig. 5). To isolate the environmental signal from background genomic differentiation, a partial Redundancy Analysis (pRDA) was performed, controlling for the first two principal components of population structure (*C. boryana* vs. *C. borbonica*). The pRDA confirmed that the bioclimatic variables remain significant drivers of genomic variation independent of species-level divergence (ANOVA: df = 5, F = 7.291, $P = 0.001$). After accounting for population structure, the environmental predictors explained an adjusted proportion of 8.32% ($R^2_{adj} = 0.0832$) of the remaining genetic variance (*SI Appendix*, Fig. S21). The pRDA ordination (*SI Appendix*, Fig. S21) revealed a shift in the relative distribution of the two species compared to the standard RDA (Fig. 5). While the high-altitude individuals of *C. borbonica* (occupying a distinct ecological niche) clustered more centrally within the environmental space, the more widespread and more

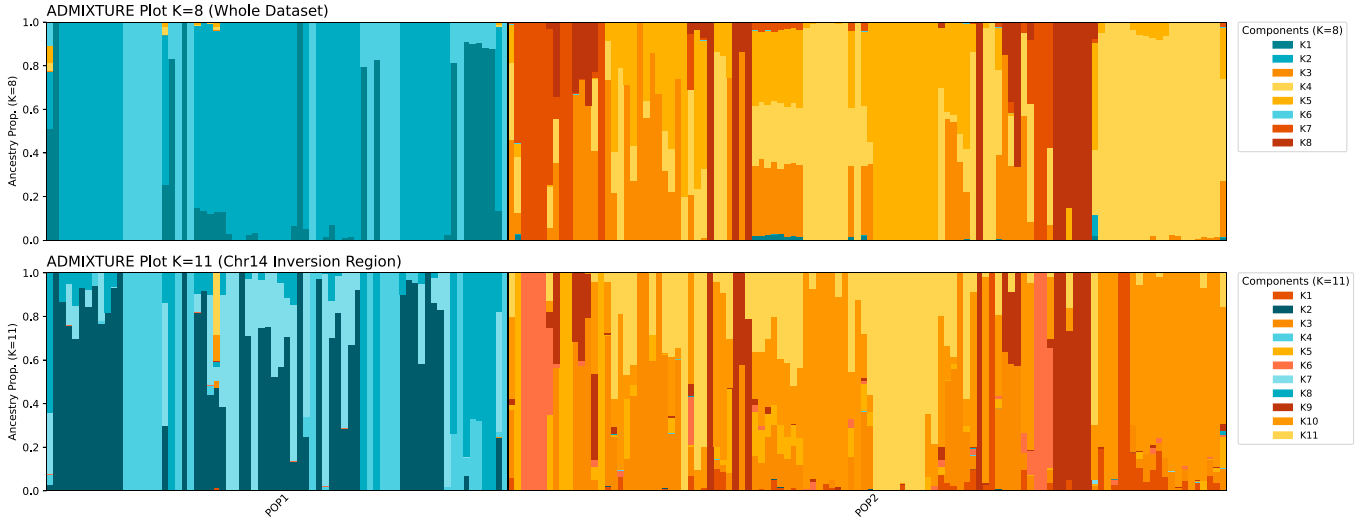

Fig. 4. On the top, results from the Admixture analysis on 184 samples and 827,809 independent SNPs applying LD across the whole genome and with K = 8. On the bottom, results from the Admixture analysis on 184 samples and 4,542 independent SNPs applying LD from major inversion in chromosome 14 and with K = 11.

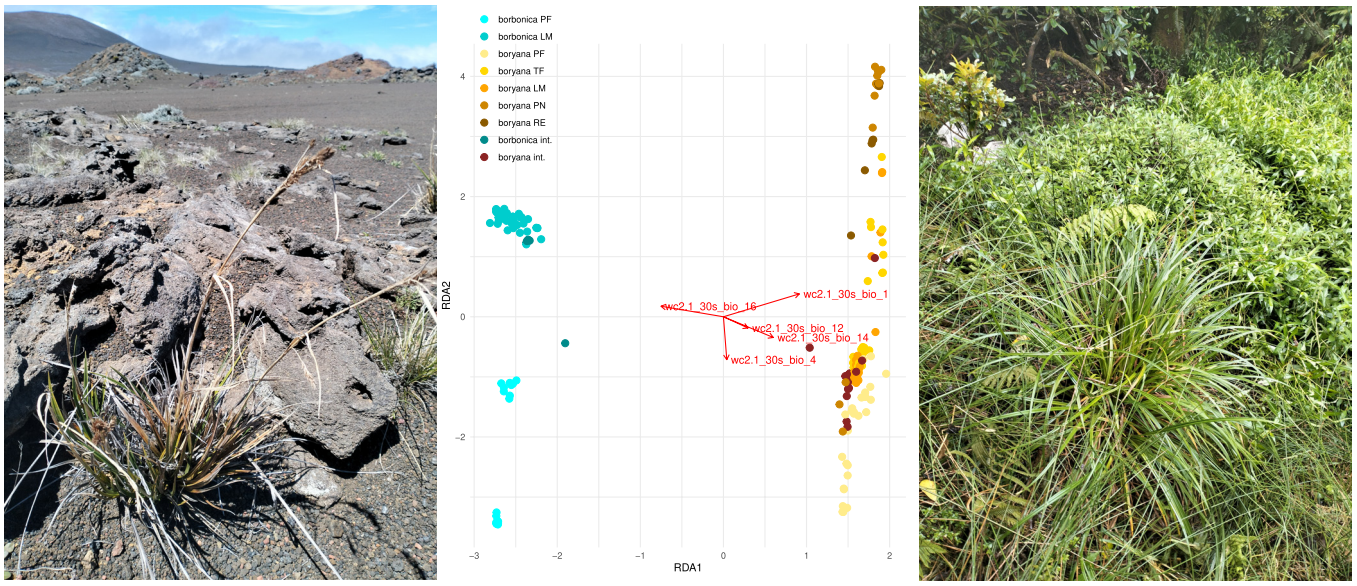

Fig. 5. Individuals of *C. borbonica* and of *C. boryana* located in the bidimensional space of RDA1 and RDA2 from the RDA analysis of 5,000 loci randomly selected across the whole genome. The signals (strength and direction) in this space of the six bioclimatic variables are shown with red arrows. Individuals are represented by dots with pure *C. borbonica* in cyan tonalities depending on the area of origin (from lighter to darker: borbonica PF = *C. borbonica* from the area of Piton de la Fournaise, and borbonica LM = *C. borbonica* from the area of Le Maïdo), introgressed *C. borbonica* in dark cyan, pure *C. boryana* in orange tonalities depending on the area of origin (from lighter to darker: boryana PF = *C. boryana* from the area of Piton de la Fournaise, boryana TF = *C. boryana* from the areas of Foret du Tevelave and Fenêtre des Makes, boryana PN = *C. boryana* from the area Piton des Neiges, boryana RE = *C. boryana* from the area Réserve Naturelle de la Roche Écrite, and boryana LM = *C. boryana* from the area of Le Maïdo) and introgressed *C. boryana* in dark brown.

ecologically flexible *C. boryana* exhibited a broader spread across the RDA axes.

Chromosomes containing large SVs that showed heightened per-window F_{ST} (INV14.1, INV18.2, INV20.3, INV3.4, INV32.16 and INV28.23), displayed also a significant relationship between genetic variation and the selected bioclimatic variables in standard RDA models (ANOVA: df = 5, F = 19.57 to 25.93, $P < 0.001$ across all chromosomes). The same highly significant result was obtained when the pRDA analysis was controlled for the first two principal components of population structure (ANOVA: df = 5, F = 7.46 to 8.33, $P < 0.001$). The analyses revealed a strong and consistent pattern across several chromosomes. For chromosome 14, the major inversion region INV14.1 showed a highly significant elevation for both selection metrics, with RDA1 magnitude being significantly higher inside the rearrangement ($P < 0.0001$) and per-SNP F_{ST} similarly increased ($P < 0.0001$) (Fig. 6). This result was mirrored on chromosome 20 (|RDA1|: $P < 0.0001$; per-SNP F_{ST}: $P < 0.0001$), where the environmental divergence signal and the overall differentiation were significantly concentrated within INV20.3. INV3.4 (|RDA1|: $P = 0.0505$; per-SNP F_{ST}: $P = 0.0979$) and INV28.23 (|RDA1|: $P = 0.0573$; per-SNP F_{ST}: $P = 0.0113$) showed marginal association with high values of |RDA1|. In INV18.2, per-SNP F_{ST} ($P = 0.2205$) and RDA1 magnitude ($P = 0.2977$) were not significant (*SI Appendix*, Figs. S13–S17), which was also true for INV32.16 (per-SNP F_{ST} $P = 0.0766$, RDA1 magnitude $P = 0.1251$) (*SI Appendix*, Figs. S22–S26). Conversely, in the pRDA, controlling for species structure, this localized enrichment disappeared entirely across all six SVs (Mann–Whitney *U*, all $P > 0.99$).

Purifying, Positive and Neutral Evolution. Analysis of aggregate evolutionary rates for genes within inversions across six chromosomes revealed heterogeneous but clear signatures of altered selection and/or drift. SVs in three different chromosomes (INV14.1, INV18.2, INV32.16) exhibited the strongest evidence for a Hill–Robertson effect: The selection pressure ($\omega = d_N/d_S$) was significantly elevated inside inversions (ranging from 1.31× to 2.11× higher than outside, $P_{INV14.1} = 0.01211$, $P_{INV18.2} < 1 \times 10^{-5}$ and $P_{INV32.16} = 0.00354$), while the corresponding neutral substitution rate (P4D) showed no significant difference ($P > 0.1$) (Table 2). This pattern suggests that high LD (reduced recombination) within these inversions compromises the efficacy of purifying selection, leading to the accumulation of potentially disadvantageous, or advantageous, mutations. In contrast, INV3.4 displayed a dramatically different signature: While the ω was near neutral (1.03×) and nonsignificant ($P = 0.114$), the neutral rate P4D was significantly increased inside the inversion (3.68×, $P < 1 \times 10^{-6}$). INV20.3 shows a similar pattern than chr3 (ω $P = 0.19442$, PD4 $P = 0.0175$). The results for INV28.23 were inconclusive, likely due to small sample sizes ($N_{genes} = 3$) (Table 2). To ensure these aggregate signatures were not driven by individual genes, we further analyzed the distribution of evolutionary rates at the individual gene level (although a high % of genes are filtered out because d_S or/and d_N are smaller than 0.01). These results (*SI Appendix*, Table S8), including shifts in median ω and P4D values and nonparametric distribution tests for the larger structural variants, suggest that the observed relaxation of purifying selection is not driven by a few genes.

GO Enrichment. The Gene Ontology (GO) enrichment analysis of the genes in the INV14.1 (with significant RDA1 and reduced purifying selection signals) revealed several highly significant biological annotations (*SI Appendix*, Fig. S27). The most significant enrichment was observed for Molecular Functions (MF), dominated by terms related to ion channel function. Specifically, mechanosensitive monoatomic ion channel activity was the most significant term across all domains ($P = 1.2 \times 10^{-8}$) and an Enrichment Factor of 0.33. This molecular theme was strongly supported by related terms for general channel activity and gated channel activity ($P < 4.0 \times 10^{-6}$). In the Biological Process (BP) domain, highly enriched terms focused on cellular structure and development, including mitochondrion organization ($P < 0.001$) and a cluster of terms related to cell projection morphogenesis and neuron development (highest BP Enrichment Factor of 0.20). The Cellular Component (CC) category was led by cell junction ($P = 0.0053$), highlighting

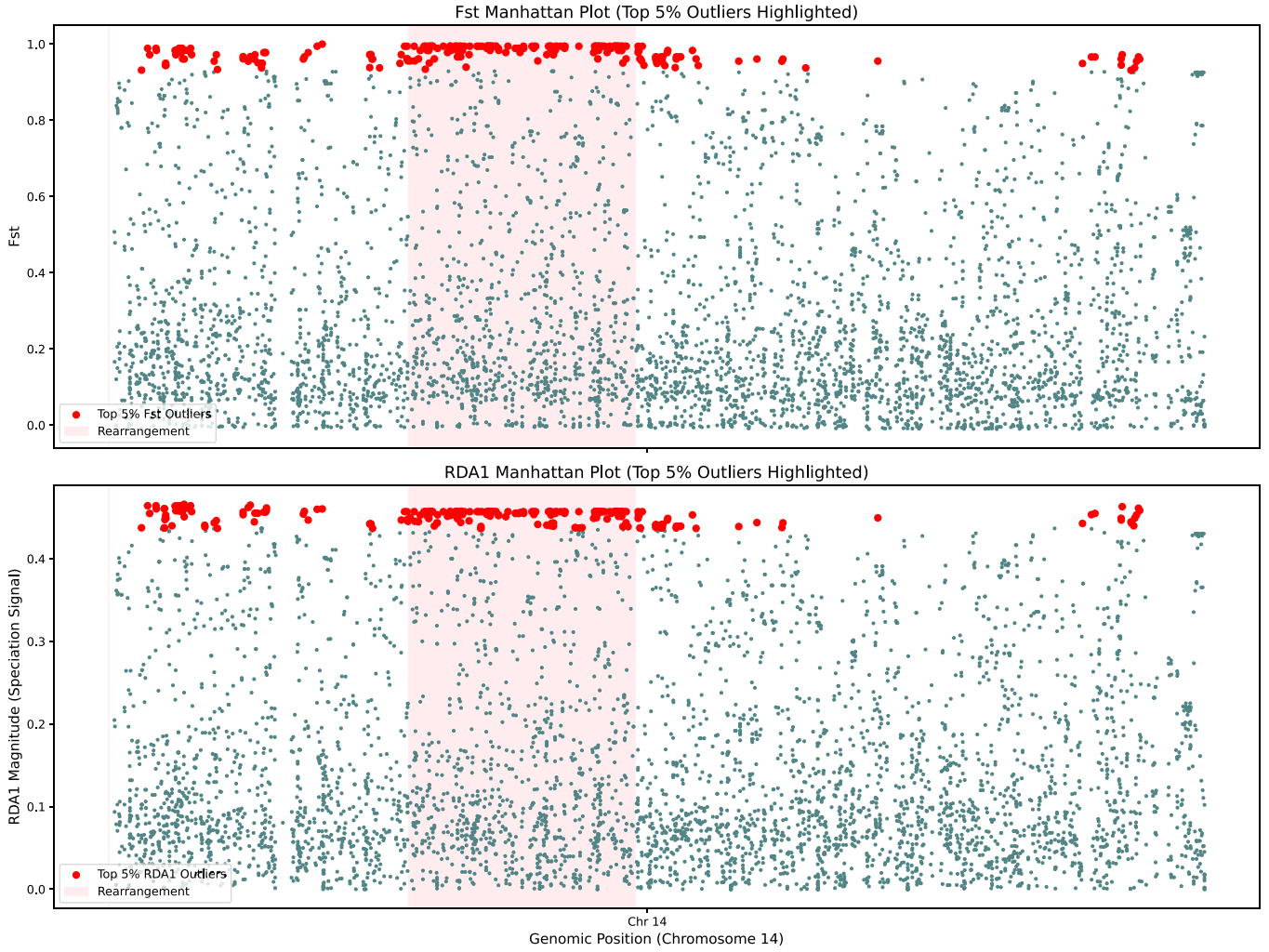

Fig. 6. Manhattan plot showing population differentiation (F_{ST}) between *C. boryana* and *C. borbonica* and |RDA1|, and its association with structural variation. F_{ST} (top) and |RDA1| (*bottom*) values of 5,000 randomly selected loci across chromosome 14 (the major inversion in this chromosome is shown with a semitransparent red window). The top outliers (1%) loci for F_{ST} and |RDA1| are shown in red.

structural components critical for cell-to-cell communication and symplastic transport.

Gene Ontology enrichment analysis of five chromosomal inversions reveals highly distinct functional specializations across the genome: INV18.2 and INV32.16 govern complementary aspects of the cell's processing and structure, with INV18.2 managing vesicle transport and cell division (top term: intra-Golgi vesicle-mediated transport, $P = 9.4 \times 10^{-11}$) and INV32.16 managing posttranslational protein modification and epigenetic regulation (peptidyl-amino acid modification, $P = 0.0037$), converging functionally only at the Golgi apparatus; meanwhile, the other inversions are specialized for different fundamental processes, as INV20.3 is heavily focused on metabolism and growth rate regulation (NADPH regeneration, $P = 0.0069$), INV3.4 is fundamentally associated with gene expression control (mRNA processing, $P = 0.00042$), and INV28.23 chromosome 28 demonstrates a powerful signature of plant development and hormone regulation (regulation of auxin polar transport, $P = 0.0062$) (*SI Appendix*, Figs. S27–S32).

Discussion

Genomic Inversions as Evolutionary Accelerators: Architecture-Driven Relaxation of Constraint. The rate at which divergence can overcome homogenizing gene flow fundamentally constrains speciation (46, 47). Mechanistically, speciation can be viewed as the evolution of restrictions to recombination (29), where chromosomal rearrangements can drive speciation by suppressing recombination (27, 48). Our work supports this scenario, suggesting that specifically large inversions do not only protect genomic regions linked to adaptation but affect the evolutionary rate of the genes they encompass resulting in divergence.

Theory suggests that inversions need to capture multiple loci necessary for local adaptation to contrasting environments (49). The most striking evidence for the resulting evolutionary mechanism in our *Carex* system is the observation that genes located within some of the largest SVs exhibit significantly higher rates of evolutionary change than genes in the collinear genome (Table 2). Crucially, this elevation in ω is suggestive of a relaxation of purifying selection, which appears to be a major driver alongside potential positive selection. The non-necessary consistency in the neutral substitution rate (fourfold degenerate sites, P4D, Table 2) across these regions supports the interpretation of a shift in selective efficacy, driven by nonsynonymous accumulation, rather than being solely an artifact of demography or ancestral polymorphism (50). This is because demographic events (like bottlenecks) or deep ancestral history would increase both neutral (P4D) and nonsynonymous substitution rates (51). Our observation of a localized increase in ω alongside a stable P4D suggests a reduction in selective efficacy specifically affecting protein-coding sites. Chromosomal inversions can therefore act as genomic accelerators, potentially

Table 2. Summary of the aggregate selection pressure (ω) and the neutral substitution rate (P_{4D}) for genes Inside (In) and Outside (Out) the inversion regions

SVID	ω or P_{4D}	In or out	N gene	d_N or sites 4D	d_S or subs. 4D	Agg. value	Ratio in/out	*P*
INV14.1	ω	In	106	0.0052	0.0105	0.4981	1.31	0.01211
		Out	373	0.0051	0.0135	0.3805		
	P_{4D}	In	106	11,772	125	0.0106	0.94	0.5887
		Out	373	38,953	439	0.0113		
INV18.2	ω	In	43	0.0107	0.0127	0.8434	1.82	1×10^{-5}
		Out	402	0.0078	0.0168	0.4645		
	P_{4D}	In	43	5,048	57	0.0113	0.80	0.1169
		Out	402	45,401	641	0.0141		
INV20.3	ω	In	9	0.0011	0.0012	0.8459	2.68	0.19442
		Out	461	0.0057	0.0181	0.3151		
	P_{4D}	In	9	780	2	0.0026	0.20	0.0175
		Out	461	49,326	631	0.0128		
INV3.4	ω	In	6	0.0414	0.0874	0.4740	1.03	0.11419
		Out	536	0.0118	0.0255	0.4617		
	P_{4D}	In	6	697	48	0.0689	3.68	4×10^{-21}
		Out	536	59,418	1,111	0.0187		
INV32.16	ω	In	6	0.0054	0.0061	0.8927	2.11	0.00354
		Out	331	0.0089	0.0211	0.4240		
	P_{4D}	In	6	651	7	0.0108	0.69	0.4152
		Out	331	32,884	510	0.0155		
INV28.23	ω	In	3	0.0008	0.0046	0.1772	0.65	1.00000
		Out	451	0.0058	0.0214	0.2731		
	P_{4D}	In	3	0.0062	161	1	0.45	0.6269
		Out	451	50,003	690	0.0138		

The Significance (P) refers to the Chi-Squared test performed on the total aggregated substitution counts. *P*-values are not corrected for multiple testing. SVID indicates type of SV (INV = inversion, DUP = duplication, TRANS = translocation, INVDP = inversion and duplication, INVTR = inversion and translocation), chromosome number and SV ranking size number (for example: INV14.1 mean an inversion in the chromosome 14 that is number 1 in the ranking of SV size).

lifting the functional "speed limit" on divergence. Acceleration is likely the consequence of suppression of recombination (29): heterozygous inversions mechanically suppress recombination within the rearranged region, creating vast compartments of increased linkage disequilibrium (LD). The genomic consequence of this suppressed recombination is often a reduction in the efficacy of purifying selection (52, 53). This effect is evidenced by the intraspecific contrasts: Genetic diversity (π) is significantly smaller within the inversions than outside, particularly in *C. borbonica* (Table 1). A reduction in π is expected under strong linked selection—specifically, background selection—acting in high LD compartments (54). While the initial fixation of a haplotype during inversion formation creates a bottleneck, the persistent reduction in π that we observe suggests that diversity is being suppressed by ongoing linked selection rather than failing to recover from a historical founder event (55). Critically, this intraspecific pattern of reduced π is consistent with being the mechanistic precursor to the interspecific pattern of higher ω (suggesting relaxed constraint) (56). By preventing selection from efficiently purging slightly deleterious mutations when comparing both species, inversions may allow the accumulation of such variants (28). This accumulation reduces selective efficacy, which is directly reflected in the increased ω ratio. This observation of relaxed constraint accompanied by reduced linked diversity, derived from comparing F_{ST}, π, and ω, mirrors findings in other model systems, such as in *Mimulus guttatus*, where an inversion is key to the adaptive divergence between coastal perennial and inland annual ecotypes (56), suggesting a conserved mechanism of evolutionary acceleration. While recombination occurs normally within homozygous arrangements of each species, the localized relaxation of purifying selection we observe (elevated ω) is likely driven by the synergy of suppressed recombination in hybrids and linked selection during adaptive sweeps (49). Within these high-LD compartments, Hill–Robertson interference reduces the efficacy of selection (57), allowing slightly deleterious mutations to accumulate more readily than in the collinear genome.

While our LD decay analyses provide evidence for recombination suppression within the respective structural variants (49), we recognize that inversions may contribute to divergence through multiple, interacting evolutionary processes (58). The observed patterns of elevated F_{ST}, reduced π, and elevated aggregate ω could theoretically also be influenced by demographic history or historical contingency (58, 59). However, the localized nature of these signatures—restricted to the inversion boundaries rather than distributed genome-wide—argues against purely demographic causes, such as a species-wide bottleneck, which would affect the collinear genome equally. Instead, within these inversions, reduced recombination interacts synergistically with linked selection. The significant reduction in nucleotide diversity (π) that we observe is consistent with background selection, where the continuous purging of deleterious alleles removes linked neutral variation in low-recombination regions (59). Simultaneously, positive directional selection (genetic hitchhiking) acting on the locally adapted ecological alleles captured by the inversions can rapidly drive these blocks to high frequency, further reducing internal diversity and inflating divergence relative to the collinear genome (60). Thus, while these evolutionary forces operate collectively, the suppression of recombination—acting in synergy with hitchhiking and background selection—is probably the primary mechanism responsible for the distinct, localized patterns of ecological divergence we observe.

Structural Variants Drive Ecological Speciation Across the Climatic Gradient. The accelerated evolutionary rate within rearrangements (Fig. 3 and *SI Appendix*, Figs. S12–S17) provided the necessary fuel for the rapid ecological speciation observed in *Carex* across the heterogeneous landscape on Réunion Island. The two species occupy dramatically contrasting environments; with *C. boryana* being restricted to continuously wet, mesic habitats, while *C. borbonica* dominates habitats characterized by higher aridity and seasonality (Figs. 5 and 6). This pattern of divergence across opposing moisture regimes is consistent with ecological speciation and has been observed for other plants in volcanic insular systems (61, 62).

Our landscape genomics analysis (Fig. 5) directly links three SVs to ecological adaptation (Fig. 6 and *SI Appendix*, Figs. S22–S26), where our bioclimatic data accounts for almost 40% of the observed genetic variation, completely separating the two species. *Carex boryana* aligns with high annual temperature and precipitation, while *C. borbonica* is driven by precipitation of the driest month. The genes encompassed within these regions are therefore evolving faster also in response to the strongest axes of divergent ecological selection (Tables 1 and 2). This ecotypic divergence is a common pattern driven by inversions, which facilitate major life-history shifts and contribute to the formation of multiple reproductive barriers (63, 64).

Population genetic structure (Figs. 2 and 4) further suggests that these regions are key drivers for maintaining reproductive isolation. While the genome-wide analysis reveals limited, low-level gene flow across several individuals, the largest inversion shows significantly less admixture, being a nearly complete barrier to gene flow (Fig. 4, although the effect may depend on the size of the inversion, see *SI Appendix*, Fig. S19). Our multiscale differentiation analysis (Table 2 and *SI Appendix*, Figs. S4 and S5) reveals that while inversions consistently accelerate protein evolution, the resulting population-level differentiation (F_{ST}) varies across genomic compartments. This dissociation suggests a tiered evolutionary process: Structural rearrangements first facilitate localized functional shifts via the relaxation of purifying selection, while the transition to a high-differentiation genomic "lock" occurs subsequently (46). This explains why some inversions (e.g., INV3.4) remain porous "vessels for introgression" (65) while others (e.g., INV14.1) achieve near-fixation, demonstrating that structural variants actively dictate the speed and permeability of the speciation process. The presence of individuals displaying approximately 50% mixed ancestry within INV14.1 and INV18.2 is highly remarkable, identifying them as putative heterozygotes for the alternative chromosomal arrangements. These regions therefore seem to segregate as Mendelian blocks. This is further exemplified by INV3.4, where the absence of diffuse background admixture confirms that the inversion remains an intact genomic unit even when moving across species boundaries. Notably, the localized introgression signal within INV3.4 suggests that it may act as a candidate vessel for adaptive introgression, where a recombination-suppressed block crosses species boundaries and is retained due to its potential adaptive value, though further experimental evidence is required to confirm selection on this specific haplotype (66). This increased overall genetic divergence within chromosomal inversions, compared to the background of a "leaky" genome, is paralleled in other key systems (33, 63), contrasting with systems where genomic islands are more porous (67). Ultimately, these findings suggest that large structural variants act as crucial genomic "locks" that protect species boundaries, allowing divergence to persist even as the rest of the genome remains permeable to introgression. This dynamic also explains the contrasting results between our standard and partial RDAs. While the standard RDA shows environmental adaptation concentrated within these SVs, controlling for species structure erases this localized enrichment. This decoupling is consistent with theoretical expectations of chromosomal speciation (49, 63, 68): If an inversion captures locally adapted loci, those alleles can rapidly become associated with the species boundary itself. As highlighted in recent landscape genomic frameworks (69), mathematically partialling out population structure under these conditions inevitably obscures the true adaptive signal, when demographic isolation and ecological divergence are inherently aligned.

The functional consequences of this accelerated divergence are highly relevant to water management in xeric environments as revealed by our GO enrichment analysis (*SI Appendix*, Figs. S27–S32). The utility of such functional annotation is well established in plant genomics, providing a robust framework for bridging the gap between large-scale genomic variation and specific physiological adaptations to environmental stress (70). Here, genes within the INV14.1 (*SI Appendix*, Fig. S27) and INV20.3 (*SI Appendix*, Fig. S30) identified significant categories strongly related to osmotic regulation and root morphology. Specifically, the INV14.1 is enriched for mechanosensitive ion channels, which regulate turgor and osmotic stress, while INV20.3 is primarily linked to metabolism and growth rate regulation. These findings align with broader functional genomic surveys where GO enrichment has been critical in dissecting the complex genetic architecture of drought tolerance, consistently identifying osmotic adjustment and root system architecture as primary evolutionary targets (71). These findings link structural genomic changes to key physiological adaptations and parallel the use of GO enrichment to define adaptive syndromes—such as the "island syndrome"—in other island radiations (22). Chromosome rearrangements such as genome duplications (72) and also inversions (66, 73, 74) are directly implicated in the rapid specialization of mechanisms controlling cell volume, nutrient uptake and osmotic balance—essential functions for adaptation to the severe and highly seasonal water stress as experienced by *C. borbonica*. While the relaxation of purifying selection (elevated ω) appears to be a broad property of the high LD and low-recombination environment created by the inversions, our GO enrichment analysis highlights specific functional consequences. The clustering of genes related to osmotic regulation and root morphology within these variants suggests that inversions effectively "locked" coadapted alleles for the physiological shift to aridity in *C. borbonica*, paralleling major adaptive inversions identified in other systems (63, 75). Our comparative genomic analysis reveals that the majority of encompassed genes are orthologous and maintain the same relative gene order, just in inverted orientation, between species. This suggests that these inversions captured preexisting, functionally related gene clusters that were in close proximity in the ancestral genome, rather than gathering them through subsequent translocations or gene duplications. Once captured, suppression of recombination within the inversion locked these existing coadapted complexes into a supergene, driving the observed functional enrichment.

General Implications: Localized vs. Genome-Wide Relaxation in Island Evolution. Finding evidence consistent with relaxed constraints, rather than exclusively widespread strong positive selection, dominates the evolutionary trajectory within these potential newly formed supergenes (e.g., in INV14.1, INV18.2 or INV32.16, Table 2). This proposes a generalizable pathway where SVs act as evolutionary accelerators, locally determining the rate of divergence likely by modulating local efficacy of purifying selection. Recent, comprehensive reviews corroborate the increasing recognition that SVs are key to speciation, but their mechanisms are diverse and often interact (28). The importance of recombination suppression is recognized in speciation genomics,

where linking this mechanism unequivocally to species origin has remained a key challenge (34, 48, 76).

The *Carex* system on Réunion Island provides a crucial empirical demonstration of the role of chromosomal inversions in accelerating rates of genetic evolution (Figs. 3 and 4 and Tables 1 and 2), driving ecological diversification (Figs. 5 and 6, *SI Appendix*, Fig. S27), and speciation. Crucially, the holocentric nature of *Carex* chromosomes likely provides a unique evolutionary advantage in this process, as the lack of localized centromeres facilitates the retention of large-scale rearrangements that might otherwise be lost due to meiotic segregation errors (36). The increased rate of karyotypic evolution typical for many holocentric lineages (77, 78) suggests that these inversions may have been part of a standing variation of chromosomal polymorphisms or arose rapidly during the colonization of new niches. In this context, chromosomal speciation is defined by the selective recruitment of rearrangements that capture suites of ecologically relevant loci. By shielding these coadapted complexes from recombination (28), the structural variants allow localized adaptation to outpace the homogenizing effects of gene flow. The holocentric resilience to structural rearrangements allows inversions to bypass the typical "underdominance paradox" (36) and persist long enough to accumulate the signatures of relaxed constraints we observe. This dynamic is further amplified by the unique recombinational landscape of holocentric organisms. While *Carex* lineages maintain high overall genome-wide recombination rates driven by the independent assortment of their numerous small chromosomes, their intrachromosomal recombination is inherently restricted, typically limited to a single crossover per bivalent (79). Because intrachromosomal recombination is already low, a single inversion can easily lock a multigenic segment into a supergene. While the rest of the genome constantly shuffles, these protected blocks allow beneficial, coadapted alleles to accumulate rapidly, significantly accelerating ecological divergence.

These findings offer a sharp contrast to other island systems. For instance, Darwin's giant daisy, *Scalesia atractyloides*, shows a genomic basis for the island syndrome characterized by signatures of selection across genes related to growth, development, and adaptation to salinity, linked to an allotetraploid history (22). The Orkney vole (*Microtus arvalis*), a continent-island speciation system, experienced a genome-wide relaxation of purifying selection (elevated d_N/d_S ratios) and reduced diversity, largely driven by pervasive genetic drift following a founder event (80). In stark contrast, our *Carex* species maintain high selective efficacy across the majority of their genome, where increased linkage disequilibrium (consistent with recombination suppression) occurs within inversions acting as local compartments of relaxed constraint. By mitigating the fitness costs typically associated with karyotypic shifts (36), holocentricity can thus permit rapid, localized adaptation under strong divergent selection without compromising the overall fitness of the nonrearranged genome. This is particularly relevant to plant speciation, where evidence linking chromosomal rearrangements to genetic and morphological differentiation at microevolutionary scales is growing, but the bridge to macroevolutionary patterns remains an active area of research (34, 76).

Ultimately, our study supports the critical role of genomic architecture as a key determinant of evolutionary speed and an important component of the speciation toolkit in diverse island and mainland systems. This conceptual framework has broad implications for understanding adaptation in the face of rapid environmental change as selection from standing genetic variation encompassed within SVs can promote rapid adaptation (81).

Materials and Methods

The genomes of *Carex boryana* and *C. borbonica* were sequenced using PacBio HiFi and scaffolded to chromosome-level assemblies using Arima Hi-C data. Structural variants were identified via comparative synteny using SyRI and validated with reciprocal Hi-C contact maps. We performed whole-genome resequencing on 184 individuals to assess population structure, linkage disequilibrium decay, and localized introgression using Patterson's D and fd statistics. Landscape genomic associations were modeled using partial Redundancy Analysis (pRDA) to disentangle climate adaptation from species-level divergence. Finally, evolutionary rates ($\omega = d_N/d_S$) were calculated for genes inside and outside major structural variants, followed by Gene Ontology enrichment. Detailed protocols for all analyses, including genome annotation and filtering parameters, are provided in the *SI Appendix, Supplementary Materials and Methods*.

Data, Materials, and Software Availability. Genomic data and custom code/scripts data have been deposited in NCBI (BioProject/BioSample) (82) and Zenodo (83). Raw sequencing data and associated metadata have been deposited in the NCBI database under BioProject ID PRJNA1464375. BioSample Accessions include SAMN59706852–SAMN59707043 https://www.ncbi.nlm.nih.gov/bioproject/PRJNA1464375 (*Carex borbonica*, *Carex boryana*, *Carex laevigata*, and *Carex helodes*) (82). Raw FASTQ reads and genome assemblies are linked to this BioProject (82). All custom code and analysis scripts have been permanently archived via Zenodo (DOI: https://doi.org/10.5281/zenodo.21699949, (82)). Study data are included in the article and/or *SI Appendix*.

ACKNOWLEDGMENTS. Project PID2024-157198NB-I00 funded by MICIU/AEI/10.13039/501100011033 and FEDER, EU. This study has been fundamentally funded by the Leonardo fBBVA LEO23-2-9663-CMT-CMA-11 (M.E. as PI). I.G.-R., R.S.-V., and M.E. have been supported by the project DiversiChrom of AEI-MICIN (PID2021-122715NB-I00). I.G.-R., R.S.-V., M.L., and M.E. have been supported by Biogenics of AEI-MICIU (PID2024-157198NB-I00). I.G.-R. has been supported by the Andalusian Regional Ministry of Economy, Knowledge, Business and University (PREDOC-00632). M.E. is truly thankful to Katty Cavero and to Keanu EC for accompanying him to the field expedition where most of the materials included in this study were collected. Moreover, we also thank Samuel Guerra-Cárdenas, Manuel J. García-Pérez, and Manuel Guzmán for helping during the collection of the remaining samples. We are thankful to an anonymous reviewer and Claire Mérot and the editor Loren Rieseberg for comments and suggestions that improved the initial versions of the manuscript. We thank Nafiseh Sargheini and the genome sequencing center at the Max-Planck Institute for plant breeding research, Cologne, Germany, for their support in generating the Hi-C data. A.V.M. and K.L. were supported by the SNSF grants 202869 and 220868 as well as the Fondation Pierre Mercier pour la science.

Author affiliations: [a]Department of Plant Biology and Ecology, Faculty of Biology, University of Seville, Seville 41012, Spain; [b]Botany Area, Department of Molecular Biology and Biochemical Engineering, Universidad Pablo de Olavide, Dos Hermanas Seville 41089, Spain; [c]Biodiversity Genomics Laboratory, Institute of Biology, Faculty of Sciences, University of Neuchâtel, 2000 Neuchâtel, Switzerland; [d]Conservatoire Botanique National de Mascarin, Saint-Leu, Réunion 97436, France; [e]Center for Ecological and Evolutionary Synthesis, Department of Biosciences, University of Oslo, Oslo 0316, Norway; [f]Department of Bioinformatics and Genetics, Swedish Museum of Natural History, Stockholm 104 05, Sweden; [g]SciLifeLab, Department of Bioinformatics and Genetics, Karolinska Institutet Science Park, Solna 171 21, Sweden; and [h]Department of Chromosome Biology, Insitute for Plant Breeding Research, Max Planck, Cologne 50829, Germany

Author contributions: K.L. and M.E. designed research; A.V.M. and M.E. performed research; C.L., J.I.M.-C., S.M.-B., M.L., K.L., and M.E. contributed new reagents/analytic tools; I.G.-R., R.S.-V., A.V.M., K.L. and M.E. analyzed data; and I.G.-R., R.S.-V., A.V.M., J.C., J.I.M.-C., A.M., S.M.-B., M.L., K.L., and M.E. wrote the paper.

1. D. Schluter, P. W. Pennell, Speciation gradients and the distribution of biodiversity. *Nature* **546**, 48–55 (2017).
2. M. Tietje *et al.*, Global variation in diversification rate and species richness are unlinked in plants. *Proc. Natl. Acad. Sci. U.S.A.* **119**, e2120662119 (2022).
3. J. J. Wiens, Speciation across life and the origins of biodiversity patterns. *Evol. J. Linn. Soc.* **3**, kzae025 (2024).
4. K. Theissinger *et al.*, How genomics can help biodiversity conservation. *Trends Genet.* **39**, 545–559 (2023).

5. B. C. Emerson, Speciation on islands: What are we learning? *Biol. J. Linn. Soc.* **95**, 47–52 (2008).
6. J. B. Losos, R. E. Ricklefs, Adaptation and diversification on islands. *Nature* **457**, 830–836 (2009).
7. F. J. Sulloway, Darwin and the Galapagos. *Biol. J. Linn. Soc.* **21**, 29–59 (1984).
8. A. S. Cheke, J. P. Hume, *Lost Land of the Dodo: An Ecological History of Mauritius, Réunion & Rodrigues* (A&C Black, 2008).
9. R. Kuussaari *et al.*, Extinction debt: A challenge for biodiversity conservation. *Trends Ecol. Evol.* **24**, 564–571 (2009).
10. B. H. Warren *et al.*, Islands as model systems in ecology and evolution: Prospects fifty years after MacArthur-Wilson. *Ecol. Lett.* **18**, 200–217 (2015).
11. R. J. Whittaker, J. M. Fernández-Palacios, T. J. Matthews, M. K. Borregaard, K. A. Triantis, Island biogeography: Taking the long view of nature's laboratories. *Science* **357**, eaam8326 (2017).
12. D. Schluter, *The Ecology of Adaptive Radiation* (OUP Oxford, 2000).
13. Y. Naciri, H. P. Linder, The genetics of evolutionary radiations. *Biol. Rev.* **95**, 1055–1072 (2020).
14. J. Cerca *et al.*, Evolutionary genomics of oceanic island radiations. *Trends Ecol. Evol.* **38**, 631–642 (2023).
15. P. R. Grant, B. R. Grant, Adaptive radiation of Darwin's finches: Recent data help explain how this famous group of Galapagos birds evolved, although gaps in our understanding remain. *Am. Sci.* **90**, 130–139 (2002).
16. S. Lamichhaney *et al.*, Rapid hybrid speciation in Darwin's finches. *Science* **359**, 224–228 (2018).
17. M. J. Landis, W. A. Freyman, B. G. Baldwin, Retracing the Hawaiian silversword radiation despite phylogenetic, biogeographic, and paleogeographic uncertainty. *Evolution* **72**, 2343–2359 (2018).
18. F. García-Maroto *et al.*, Δ6-Desaturase sequence evidence for explosive Pliocene radiations within the adaptive radiation of Macaronesian Echium (Boraginaceae). *Mol. Phylogenet. Evol.* **52**, 563–574 (2009).
19. M. Fernández-Mazuecos *et al.*, The radiation of Darwin's giant daisies in the Galápagos Islands. *Curr. Biol.* **30**, 4989–4998 (2020).
20. R. G. Albaladejo *et al.*, Reconstruction of the spatio-temporal diversification and ecological niche evolution of Helianthemum (Cistaceae) in the Canary Islands using genotyping-by-sequencing data. *Ann. Bot.* **127**, 597–611 (2021).
21. D. Berner, W. Salzburger, The genomics of organismal diversification illuminated by adaptive radiations. *Trends Genet.* **31**, 491–499 (2015).
22. J. Cerca *et al.*, The genomic basis of the plant island syndrome in Darwin's giant daisies. *Nat. Commun.* **13**, 3729 (2022).
23. J. Cerca *et al.*, No evidence of transposable element bursts in the Galápagos Scalesia adaptive radiation despite hybridization, diversification and ecological niche shifts. *Mob. DNA* **16**, 23 (2025).
24. A. K. Baksi, K. A. Hoffman, On the age and morphology of the Réunion event. *Geophys. Res. Lett.* **27**, 2997–3000 (2000).
25. K. Takayama, D. J. Crawford, P. López-Sepúlveda, J. Greimler, T. F. Stuessy, Factors driving adaptive radiation in plants of oceanic islands: A case study from the Juan Fernández Archipelago. *J. Plant Res.* **131**, 469–485 (2018).
26. D. A. Marques, J. I. Meier, O. Seehausen, A combinatorial view on speciation and adaptive radiation. *Trends Ecol. Evol.* **34**, 531–544 (2019).
27. L. H. Rieseberg, Chromosomal rearrangements and speciation. *Trends Ecol. Evol.* **16**, 351–358 (2001).
28. E. L. Berdan *et al.*, Structural variants and speciation: Multiple processes at play. *Cold Spring Harb. Perspect. Biol.* **16**, a041446 (2024).
29. R. K. Butlin, Recombination and speciation. *Mol. Ecol.* **14**, 2621–2635 (2005).
30. A. A. Hoffmann, L. H. Rieseberg, Revisiting the impact of inversions in evolution: From population genetic markers to drivers of adaptive shifts and speciation? *Annu. Rev. Ecol. Evol. Syst.* **39**, 21–42 (2008).
31. E. L. Berdan *et al.*, How chromosomal inversions reorient the evolutionary process. *J. Evol. Biol.* **36**, 1761–1782 (2023).
32. P. Nosil, J. L. Feder, Genomic divergence during speciation: Causes and consequences. *Philos. Trans. R. Soc. Lond. B. Biol. Sci.* **367**, 332–342 (2012).
33. A. Mackintosh *et al.*, Chromosome fissions and fusions act as barriers to gene flow between Brenthis fritillary butterflies. *Mol. Biol. Evol.* **40**, msad043 (2023).
34. C. Benítez-Benítez *et al.*, Bridging micro and macroevolution: Insights from chromosomal dynamics in plants. *Front. Plant Sci.* **16**, 1606450 (2025).
35. F. J. Ayala, M. Coluzzi, Chromosome speciation: Humans, *Drosophila*, and mosquitoes. *Proc. Natl. Acad. Sci. U.S.A.* **102**, 6535–6542 (2005).
36. K. Lucek, H. Augustijnen, M. Escudero, A holocentric twist to chromosomal speciation? *Trends Ecol. Evol.* **37**, 655–662 (2022).
37. S. Martín-Bravo *et al.*, A tale of worldwide success: Behind the scenes of Carex (Cyperaceae) biogeography and diversification. *J. Syst. Evol.* **57**, 695–718 (2019).
38. I. McDougall, The geochronology and evolution of the young volcanic island of Réunion. *Indian Ocean. Geochim. Cosmochim. Acta* **35**, 261–288 (1971).
39. M. Escudero, M. Luceño, Taxonomic revision of the tropical African group of Carex subsect. Elatae (sect. Spirostachyae, Cyperaceae). *An. Jard. Bot. Madr.* **68**, 225–247 (2011).
40. M. Escudero, M. Luceño, Systematics and evolution of Carex sects. Spirostachyae and Elatae (Cyperaceae). *Plant Syst. Evol.* **279**, 163–189 (2009).
41. J. I. Márquez-Corro *et al.*, IAPT/IOPB chromosome data 28. *Taxon* **67**, 1235–1245 (2018).
42. J. Gabriel *et al.*, BRAKER3: Fully automated genome annotation using gene prediction tools. *Genome Res.* **34**, 110–121 (2024).
43. S. Baril *et al.*, Earlgrey: A genome-wide transposable element annotation pipeline. *Mob. DNA* **15**, 1 (2024).
44. J. T. Lovell *et al.*, GENESPACE tracks regions of interest and gene copy number variation across multiple genomes. *Elife* **11**, e78526 (2022).
45. T. R. Booker, S. Yeaman, M. C. Whitlock, Variation in recombination rate affects detection of outliers in genome scans under neutrality. *Mol. Ecol.* **29**, 4274–4279 (2020).
46. J. L. Feder, S. P. Egan, P. Nosil, The genomics of speciation-with-gene-flow. *Trends Genet.* **28**, 342–350 (2012).
47. M. Ravinet *et al.*, Interpreting the genomic landscape of speciation: A road map for finding barriers to gene flow. *J. Evol. Biol.* **30**, 1450–1477 (2017).
48. R. Faria, A. Navarro, Chromosomal speciation revisited: Rearranging theory with pieces of evidence. *Trends Ecol. Evol.* **25**, 660–669 (2010).
49. M. Kirkpatrick, N. Barton, Chromosome inversions, local adaptation and speciation. *Genetics* **173**, 419–434 (2006).
50. M. A. Noor, S. M. Bennett, Islands of speciation or mirages in the desert? Examining the role of restricted recombination in maintaining species. *Heredity* **103**, 439–444 (2009).
51. G. Luikart, P. R. England, D. Tallmon, S. Jordan, P. Taberlet, The power and promise of population genomics: From genotyping to genome typing. *Nat. Rev. Genet.* **4**, 981–994 (2003).
52. S. P. Otto, N. H. Barton, The evolution of recombination: Removing the limits to natural selection. *Genetics* **147**, 879–906 (1997).
53. A. J. Betancourt, J. J. Welch, B. Charlesworth, Reduced effectiveness of selection caused by a lack of recombination. *Curr. Biol.* **19**, 655–660 (2009).
54. Y. Kim, R. Nielsen, Linkage disequilibrium as a signature of selective sweeps. *Genetics* **167**, 1513–1524 (2004).
55. T. E. Cruickshank, M. W. Hahn, Reanalysis suggests that genomic islands of speciation are due to reduced diversity, not reduced gene flow. *Mol. Ecol.* **23**, 3133–3157 (2014).
56. L. M. Kollar, L. E. Stanley, S. K. Kenchanmane Raju, D. B. Lowry, C. E. Niederhuth, The evolution of locally adaptive chromosome inversions in Mimulus guttatus. *Mol. Ecol.* **34**, e17708 (2025).
57. W. G. Hill, A. Robertson, The effect of linkage on limits to artificial selection. *Genet. Res.* **8**, 269–294 (1966).
58. K. E. Lotterhos, M. C. Whitlock, Evaluation of demographic history and neutral parameterization on the performance of F_{ST} outlier tests. *Mol. Ecol.* **23**, 2178–2192 (2014).
59. J. M. Comeron, Background selection as baseline for nucleotide variation across the Drosophila genome. *PLoS Genet.* **10**, e1004434 (2014).
60. W. Stephan, Signatures of positive selection: From selective sweeps at individual loci to subtle allele frequency changes in polygenic adaptation. *Mol. Ecol.* **25**, 79–88 (2016).
61. O. G. Osborne, T. E. Batstone, S. J. Hiscock, D. A. Filatov, Rapid speciation with gene flow following the formation of Mt. *Etna. Genome Biol. Evol.* **5**, 1704–1715 (2013).
62. N. M. Suárez, J. Pestano, R. P. Brown, Ecological divergence combined with ancient allopatry in lizard populations from a small volcanic island. *Mol. Ecol.* **23**, 4799–4812 (2014).
63. D. B. Lowry, J. H. Willis, A widespread chromosomal inversion polymorphism contributes to a major life-history transition, local adaptation, and reproductive isolation. *PLoS Biol.* **8**, e1000500 (2010).
64. C. Vangestel *et al.*, Chromosomal inversions from an initial ecotypic divergence drive a gradual repeated radiation of Galápagos beetles. *Sci. Adv.* **10**, eadk7906 (2024).
65. T. Leroy, M. Heuertz, Adaptive introgression in the context of climate adaptation. *Mol. Ecol.* **35**, e70333 (2026).
66. W. Zhang *et al.*, Genome architecture and diverged selection shaping pattern of genomic differentiation in wild barley. *Plant Biotechnol. J.* **21**, 46–62 (2023).
67. R. A. Bay, K. Ruegg, Genomic islands of divergence or opportunities for introgression? *Proc. Biol. Sci.* **284**, 20162414 (2017).
68. L. M. Blumer *et al.*, Introgression dynamics of sex-linked chromosomal inversions shape the Malawi cichlid radiation. *Science* **388**, eadr9961 (2025).
69. T. Capblancq, B. R. Forester, Redundancy analysis: A Swiss army knife for landscape genomics. *Methods Ecol. Evol.* **12**, 2298–2309 (2021).
70. S. Y. Rhee, M. Mutwil, Towards revealing the functions of all genes in plants. *Trends Plant Sci.* **19**, 212–221 (2014).
71. F. Rasool *et al.*, Transcriptome unveiled the gene expression patterns of root architecture in drought-tolerant and sensitive wheat genotypes. *Plant Physiol. Biochem.* **178**, 20–30 (2022).
72. H. Maherali, A. E. Walden, B. C. Husband, Genome duplication and the evolution of physiological responses to water stress. *New Phytol.* **184**, 721–731 (2009).
73. D. B. Lowry, R. C. Rockwood, J. H. Willis, Ecological reproductive isolation of coast and inland races of Mimulus guttatus. *Evolution* **62**, 2196–2214 (2008).
74. M. C. Hall, D. B. Lowry, J. H. Willis, Is local adaptation in Mimulus guttatus caused by trade-offs at individual loci? *Mol. Ecol.* **19**, 2739–2753 (2010).
75. M. Todesco *et al.*, Massive haplotypes underlie ecotypic differentiation in sunflowers. *Nature* **584**, 602–607 (2020).
76. K. Lucek *et al.*, The impact of chromosomal rearrangements in speciation: From micro-to macroevolution. *Cold Spring Harb. Perspect. Biol.* **15**, a041447 (2023).
77. M. Escudero, J. M. Arroyo, S. Sánchez-Ramírez, P. Jordano, Founder events and subsequent genetic bottlenecks underlie karyotype evolution in the Ibero-North African endemic Carex helodes. *Ann. Bot.* **133**, 871–882 (2024).
78. C. M. Tribble *et al.*, Macroevolutionary inference of complex modes of chromosomal speciation in a cosmopolitan plant lineage. *New Phytol.* **245**, 2350–2361 (2025).
79. F. Zedek *et al.*, Chromosome size as a robust predictor of recombination rate: Insights from holocentric and monocentric systems. *Genetics* **232**, iyaf247 (2026).
80. X. Wang, G. Heckel, Genome-wide relaxation of selection and the evolution of the island syndrome in Orkney voles. *Genome Res.* **34**, 851–862 (2024).
81. F. C. Jones *et al.*, The genomic basis of adaptive evolution in threespine sticklebacks. *Nature* **484**, 55–61 (2012).
82. I. Gómez-Ramos *et al.*, Data from "Chromosomal inversions accelerate genetic evolution and drive ecological speciation across an island gradient" NCBI BioProject. https://www.ncbi.nlm.nih.gov/bioproject/PRJNA1464375. Deposited 11 May 2026.
83. M. Escudero, Code from "Chromosomal inversions accelerate genetic evolution and drive ecological speciation across an island gradient." Zenodo. https://doi.org/10.5281/zenodo.21699950. Deposited 30 July 2026.